



Journal of Mining and Environment (JME)

journal homepage: [www.jme.shahroodut.ac.ir](http://www.jme.shahroodut.ac.ir)



## Effect of Confining Pressure on $I_s(50)$ Obtained by Point Load Test

Vahab Sarfarazi<sup>1\*</sup> and Kaveh Asgari<sup>2</sup>

1- Associate Professor, Department of Mining Engineering, Hamedan University of Technology, Hamedan, Iran

2- Research Scholar, Department of Mining Engineering, Shahid Bahonar University of Kerman, Kerman, Iran

### Article Info

Received 19 June 2021

Received in Revised form 28 July 2021

Accepted 2 August 2021

Published online 2 August 2021

DOI: [10.22044/jme.2021.10918.2070](https://doi.org/10.22044/jme.2021.10918.2070)

### Keywords

Point load test

PFC2D

Tensile crack

### Abstract

In this investigation, the impact of confining pressure on the tensile strength obtained by point load test (PLT) is examined by particle flow code in two dimensions. In this regard, at first, a numerical model is calibrated using the Brazilian experimental test results. The tensile strength of the model material is equal to 2.5 MPa. Secondly, PLT is performed on the numerical models with dimension of 15 cm × 50 cm. The rectangular models are tested by PLT under the presence of the confining pressure. The loading rate is 0.001 mm/min, confining that the pressure is changed with the 13 different values of 0 MPa, 0.002 MPa, 1MPa, 1.5 MPa, 2 MPa, 2.5 MPa, 3MPa, 3.5 MPa, 4 MPa, 5MPa, 6 MPa, 9 MPa, and 11 MPa. The results obtained show that the vertical tensile crack develops through the model under a low confining pressure, while several shear bands are developed in the models under a high confining pressure. The number of shear cracks is augmented by augmenting the confining pressure.  $I_s(50)$  is the augment by augmenting the confining pressure. Also a new criterion is rendered in order to determine  $I_s(50)$  based on the confining pressure.

## 1. Introduction

Some methods such as direct pull-on briquettes or indirect tensile and bending tests can determine the rock tensile strength. Although the most appropriate one could possibly be the uniaxial tensile test, a very stiff closed-loop servo-controlled testing system is required for the stability of the test (Basant [1]; Shah [2]). Due to the fragile nature of rocks, performing direct tensile tests is hectic; however, if it is performed accurately, it will generate a very useful data. So far there have been various modes of direct tensile tests on the cementitious specimens presented in the literature (Chen [3]; Mazars, [4]). However, these experiments had some demerits such as the lack of reliability, reproducibility, and simplicity. Thus it requires an alternative approach in order to overcome these defects. Measuring the tensile strength indirectly (Brazilian test, Double punch test DPT, 3- and 4-point bending tests, point load

test, etc.) is usually replaced by the direct uniaxial tests; this is due to the fact that (1) they are more simple and easier to use, in particular, for controlling the production of materials (for plain rock, for instance, the point load test is common and standard), and (2) the scattering results is reduced. One of the methods that satisfies the introduced requirement is the point load test (PLT). PLT is a useful and cheap testing procedure to predict the tensile and rocks compressive strengths because of the ease of specimen preparation, its simplicity of testing, and possible field application. Also it is possible to perform the point load test on the irregular specimens. The idea of examining irregular rock lumps, at first, was suggested by Protodyakonov (Protodyakonov, [5]) in Russia in 1960. Bieniawski [6] introduced the general applications of PLT. In 1964, the International Bureau for Rock Mechanics (Broch and Franklin,

✉ Corresponding author: [vahab.sarfarazi@gmail.com](mailto:vahab.sarfarazi@gmail.com) (V. Sarfarazi).

[7]) adopted PLT. Since the beginning of PLT, various schemes of correction have been represented for size over the years (e.g. Broch and Franklin [7]; Basu [8]; Basu [9]). The approach that is revised and recommended for PL testing represents repeated proposals to enhance the approach of evaluating the PL strength index (Broch and Franklin [7]; Bieniawski [6]; Singh [10]; Chau and Wong [11]; Fener et al. [12]; Sonmez et al. [13-15]; Basu and Aydin [16]; Kahraman and Gunaydin [17]; Kayabal and Selcuk [18]; Ma [19]; Heidari et al. [20]; Singh [21]; Li et al. [22]; Haeri et al. [23, 24]). The specimens can be of various shapes, and are applied to test with weak and strong rocks (Tsiambaos and Sabatakakis [25]; Heidari et al. [20]). There are diverse kinds of sample geometries and testing methods that can be applied in order to evaluate the compressive and tensile strengths under different loading conditions (Zhou et al. [26], Ayatollahi and Alborzi [27], Wei et al. [28]; Xu et al. [29]; Lee [30]; Rajabi [31]; Yaylac [32]; Lin et al. [33-37]). Correlation determination of the point of load index ( $Is(50)$ ) and the uniaxial compressive strength/tensile strength are vital points in using PLT on diverse kinds of rocks. Several experimental tests have indicated that the conversion parameters are different in igneous, metamorphic, and sedimentary rocks (Kahraman et al. [38]; Fener et al. [12]). The relationship between  $Is(50)$  and the Brazilian tensile strength is also often considered (Heidari et al. [20]). The objective of this investigation is to determine the influences of confining pressure on the point-load index  $Is(50)$ . Also a new criteria was rendered to determine  $Is(50)$  based on the confining pressure.

## 2. Point load test (PLT)

As shown in Figure 1, the conical plates apply an a slight focused compressive force on the concrete sample, and it continues till the collapse of sample due to splitting (Figure 1). An assembly consisting of the structures such as a pressure gage, a frame, and a hydraulic jack forms the system of loading. Based on the following equation, the failure load should be recorded and applied for calculation of the index of point load strength,  $Is(50)$ , (Heidari et al. [20]).

$$Is(50) = P/D_e^2 \quad (1)$$

where  $P$  is the peak load and  $D$  is equivalent to the core diameter for the diametric and other forms.

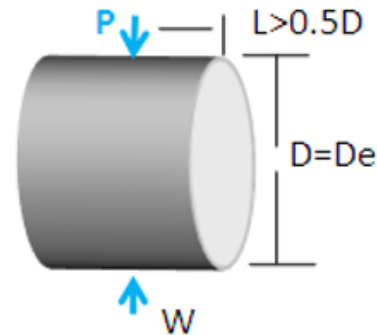


Figure 1. A schematic view of PLT.

## 3. Numerical simulation

### 3.1. Bonded particle model and particle flow code 2D (PFC2D)

PFC2D is a discrete element code that introduces a substance as a rigid particles structure, which can transfer discretely and its interaction is just at the contacts (Potyondy and Cundall [39]). Particle movements and interaction forces were calculated by a central finite difference approach (similar to the one used in DEM). In the case of contact models (either linear or non-linear) both the linear and non-linear contact models with frictional sliding can be used for the contact models. In this investigation, the linear contact model was used. An elastic relationship was established between the particle contact force and the relative displacements. Some provided routines were used for producing a parallel-bonded particle model for PFC2D. For producing this model, some micro-characteristics such as parallel-bond stiffness ratio, minimum radius of ball, ratio of stiffness  $k_n$  over  $k_s$ , ball-to-ball contact modulus, parallel normal bond strength, coefficient of ball friction, parallel bond modulus, ratio of standard deviation to mean of bond strength both in the normal and shear direction, parallel shear bond strength, and parallel bond radius multiplier must be introduced. A calibration approach is critical to establish the appropriate micro-properties for application to an assembly of particles. The tests conducted on the laboratory model samples cannot exactly determine the bonding properties and contact of particles. The characteristics of a substance that are represented by laboratory tests are macro-mechanical in nature; this is due to the fact that they

show a continuum behavior. A reverse modeling approach was applied to represent the suitable micro-mechanical characteristics of the numerical models from the macro-mechanical characteristics defined in the laboratory experiments. The trial-and-error method is an approach that can be applied to connect these two sets of material characteristic. This approach provides an estimation of the micro-mechanical characteristic quantities, and compares the properties of the strength and deformation derived from the numerical models and the laboratory specimens. Then the closest simulated macroscopic response of the micro-mechanical characteristic quantities to that of the laboratory tests is considered for the discontinuous jointed blocks.

### 3.2. Preparation and calibration of numerical model

The uniaxial compression test and the Brazilian test were applied to calibrate the compressive strength, young modulus, and sample tensile strength in the PFC2D model. The generated standard process of a PFC2D assembly to show a

test model includes four sections: (a) particles generating and packing, (b) installation of isotropic stress, (c) deletion of floated particles, and (d) installing the band. Using the micro-characteristics indicated in Table 2 and the standard approaches of calibrating (Potyondy and Cundall, [39]), a calibrated assembly of the PFC particles was provided. A Brazilian test with the diameter of 54 mm was used in the numerical tests. The sample was created by 5,615 particles. The disk was fractured by the movement of the lateral walls toward each other with a slight velocity of 0.016 m/s. Figures 2a and 2b indicate the patterns of failure of the experimental and numerical experimented specimens, respectively. Furthermore, Figure 2b depicts the particle displacement vector and the distribution of bond force. According to the results obtained, there is a well matching between numerical the simulation and experimental tests. A comparison between the experimental measurements and the numerical tensile strength is shown in Table 2. This table indicates a well accordance between the experimental and numerical results.

**Table 1. Micro-characteristics used to introduce the intact rock.**

Parameter	Value	Parameter	Value
Type of particle	disc	Parallel bond radius multiplier	1
Density	3000	Young modulus of parallel bond (GPa)	40
Minimum radius	0.27	Parallel bond stiffness ratio	1.7
Size ratio	1.56	Particle friction coefficient	0.4
Porosity ratio	0.08	Parallel bond normal strength, mean (MPa)	9
Damping coefficient	0.7	Parallel bond normal strength, SD (MPa)	2
Contact young modulus (GPa)	40	Parallel bond shear strength, mean (MPa)	9
Stiffness ratio	1.7	Parallel bond shear strength, SD (MPa)	2

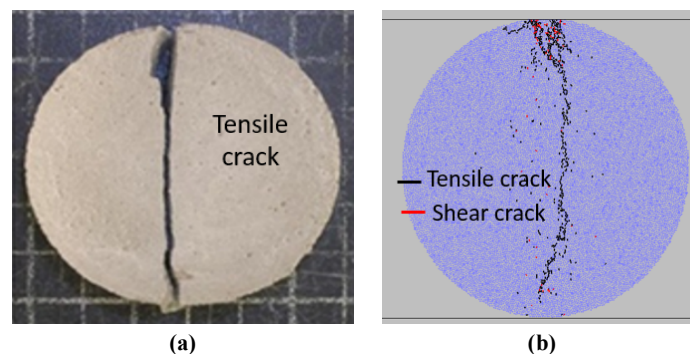


**Figure 2. Failure patterns in a) physical sample, b) PFC2D model.**

**Table 2. Brazilian tensile strength of physical and numerical specimens.**

Physical tensile strength (MPa)	2.5
Numerical tensile strength (MPa)	2.6

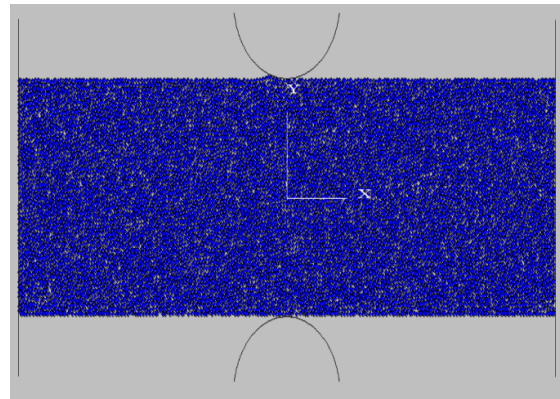
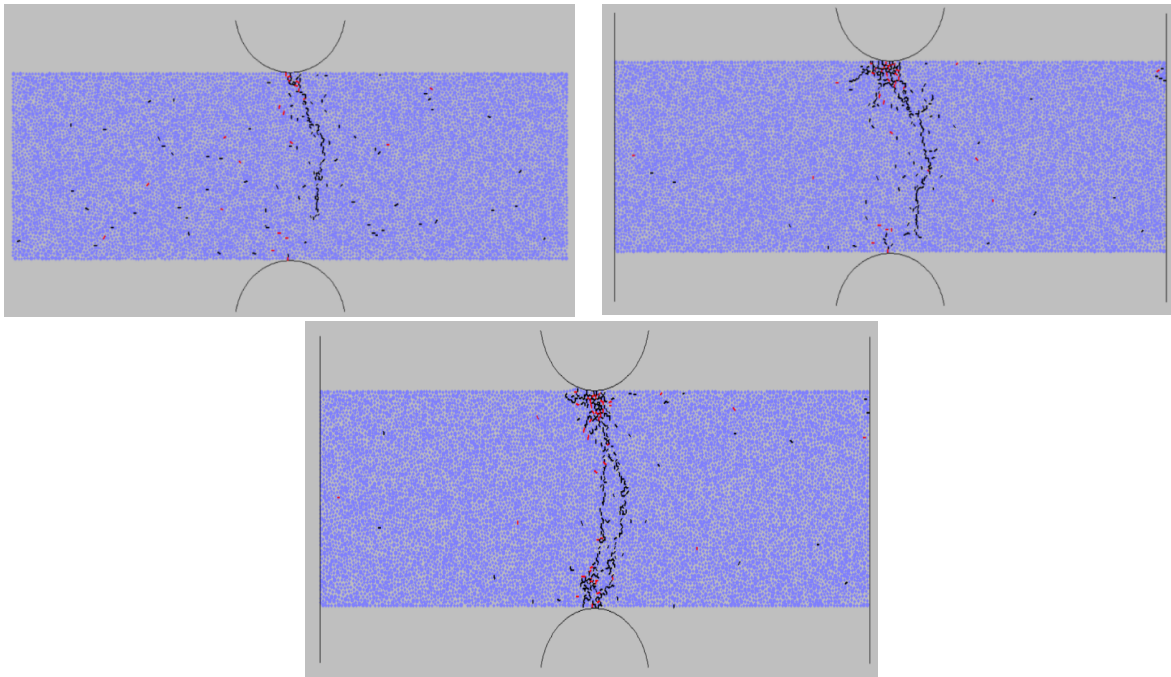
### 3.3. Preparation of model by PFC

After PFC2D calibration, PLTs were simulated by generating a rectangular model in PFC2D (by applying the calibrated micro-parameters) (Figure 3). The dimensions of the PFC sample were 15 mm x 50 mm. In order to build the rectangular sample, a number of 8,183 disks was used; the minimum radius of the disks was 0.27. The rectangular models are subjected to the confining pressures of 0 MPa, 0.002 MPa, 1 MPa, 1.5 MPa, 2 MPa, 2.5 MPa, 3 MPa, 3.5 MPa, 4 MPa, 5 MPa, 6 MPa, 9 MPa, and 11 MPa. The value of confining pressure was chosen randomly. The maximum confining pressure was nearly five times more than the value of the tensile strength. These models were loaded vertically till the failure occurred. The reaction forces on the top wall were considered and registered as the tensile forces.

### 3.4. Crack distribution in model

Figures 4, 5, 6, and 7 show the effect of confining pressure on the crack distribution in the models.

The red line and the black line are related to the shear and tensile cracks, respectively. In the case that confining pressure is less than 1.5 MPa ( $\sigma_t/2$ ), one or two vertical tensile cracks bring the model to failure (Figure 4). When the confining pressure is between 1.5 MPa and 5 MPa, the shear bands consisting of the tensile and shear cracks lead to the failure of the model (Figure 5). When the confining pressure is 6 MPa, the tensile and shear cracks are developed beneath the loading walls, and no major failure occurs (Figure 6). In these conditions, the cone penetrates in the model. In some cases, the models fail under a high confining pressure (Figure 7).

**Figure 3. A schematic view of PLT.****Figure 4. Failure pattern in PLT.**

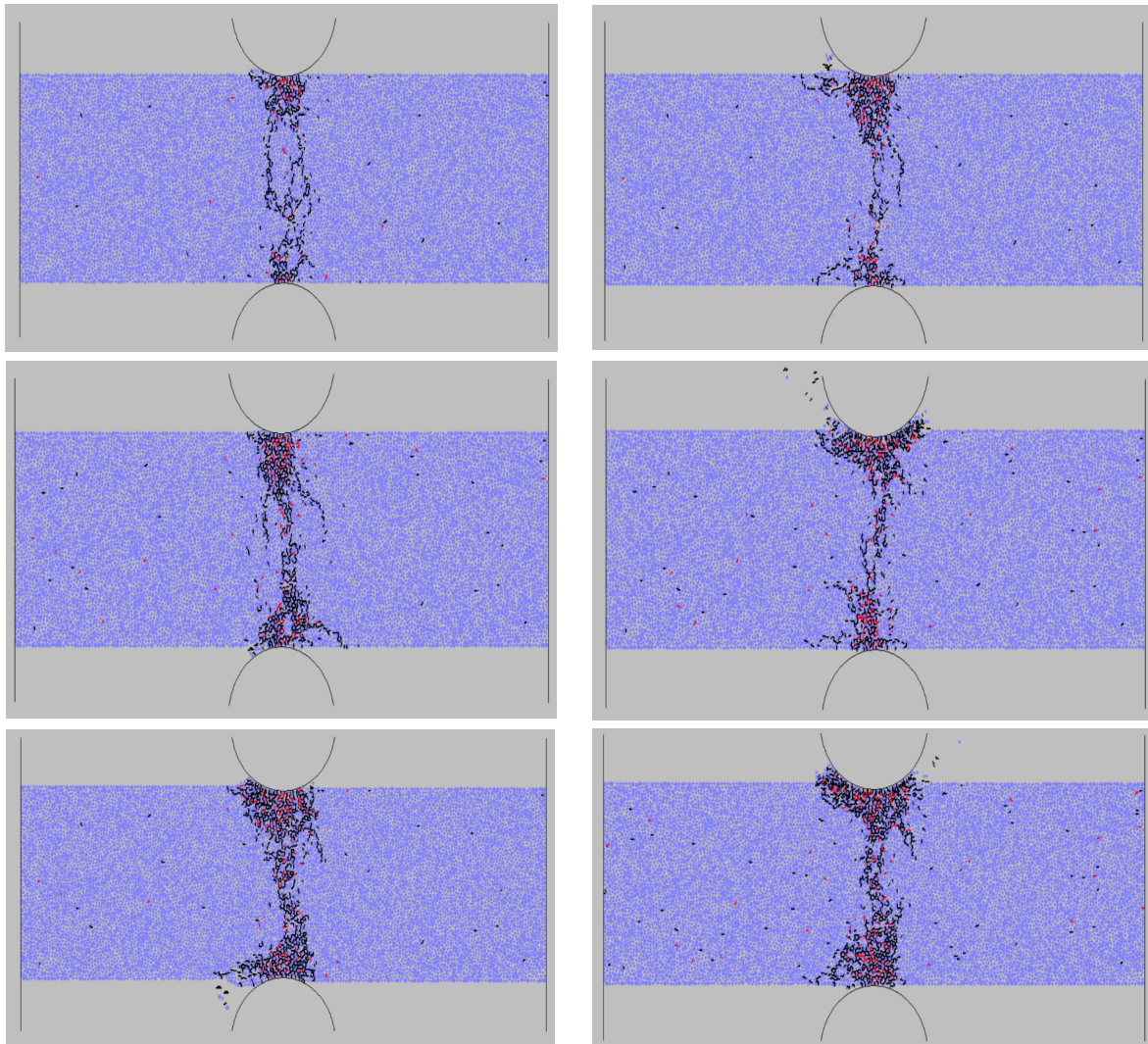


Figure 5. Failure pattern in PLT.

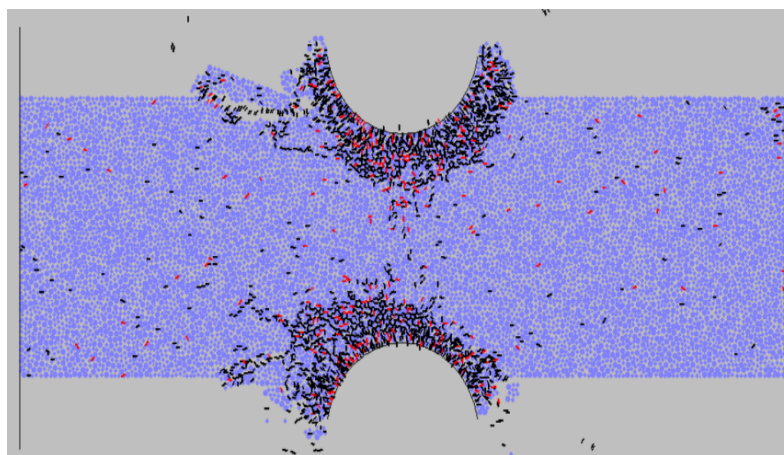


Figure 6. Failure pattern in PLT.

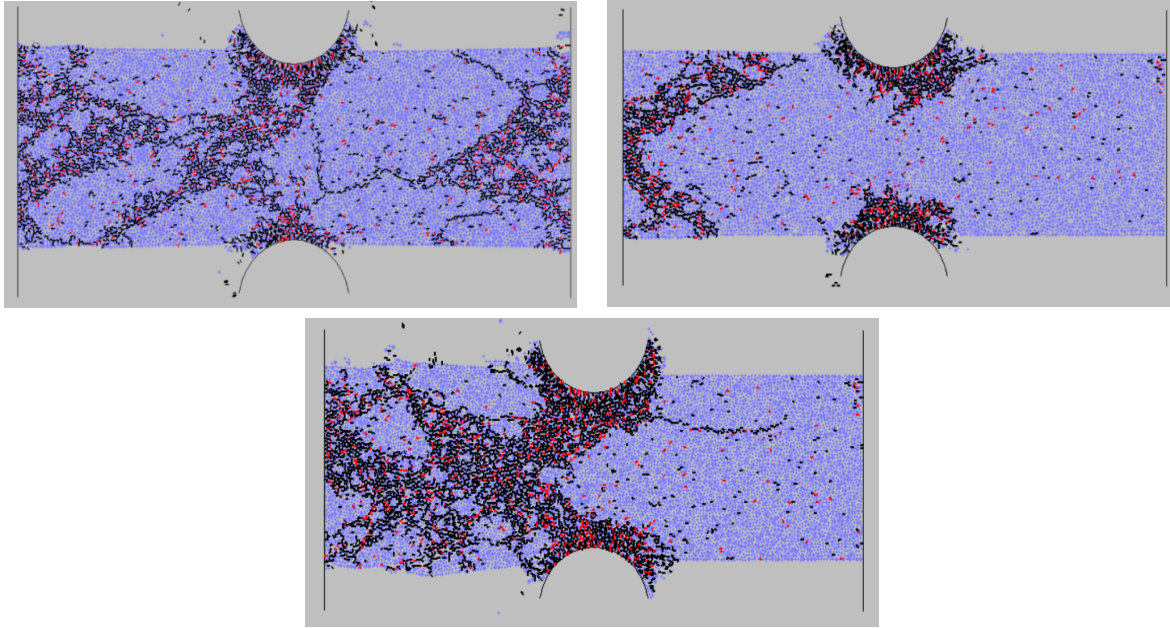


Figure 7. Failure pattern in PLT.

### 3.5. Influence of confining pressure on $I_s50$

Figure 8 shows the influence of the confining pressure on  $I_s50$ .  $I_s50$  is increased with increase in the confining pressure. The best curve fitting on these data shows that  $Y = 2.69e^{0.1105x}$ . This equation shows that when the confining pressure is zero, the tensile strength obtained by the equation is 2.69 MPa, which is a real one. Therefore, this equation can be used for measurement of  $I_s50$  when the model is under the confining pressure.

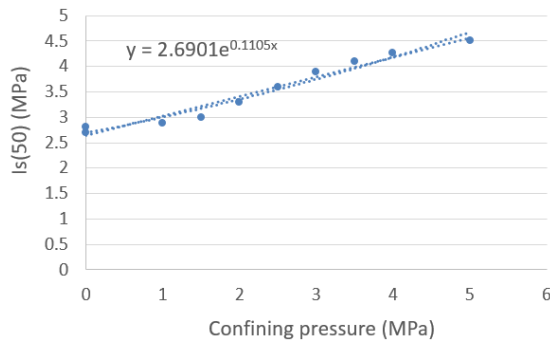


Figure 8. Influence of confining pressure on tensile strength.

The influence of lateral confinement on the PLT results has also been given by Palassi and Afzali [40]. Figure 9a shows the assembly of PLT in the presence of confining pressure. Figure 9b shows the typical failure pattern occurring in the samples. Also Figure 9c shows the effect of confining pressure on the point load index for marble. By a

comparison between Figure 8 and Figure 9c, it can be concluded that a good accordance was established between the numerical results and the experimental test.

### 4. Conclusions

In this investigation, the impact of confining pressure on the tensile strength obtained by the point load test (PLT) was examined by PFC2D. In this regard, at first, the calibration of the numerical model was conducted by the Brazilian experimental test results. Secondly, PLT was performed on the numerical models with dimensions of 15 cm × 50 cm. The rectangular models were tested by PLT under the presence of a confining pressure. The confining pressure was changed with the 13 different values of 0 MPa, 0.002 MPa, 1 MPa, 1.5 MPa, 2 MPa, 2.5 MPa, 3 MPa, 3.5 MPa, 4 MPa, 5 MPa, 6 MPa, 9 MPa, and 11 MPa. The results obtained showed that:

- The vertical tensile crack was developed through the model under a low confining pressure, while several shear bands were developed in the models under a high confining pressure. The number of shear cracks augments by augmenting the confining pressure.
- When the confining pressure is less than 1.5 MPa ( $\sigma/3$ ), one or two vertical tensile cracks bring the model to a failure. When the confining pressure is between 1.5 MPa and 5 MPa, the

shear bands consisting of the tensile and shear cracks lead to the failure of the model. When the confining pressure is 6 MPa, the tensile and shear cracks are developed beneath the loading walls, and no major failure occurs. In some cases, the models fail under a high confining pressure.

- Is50 is increased with increase in the confining pressure. The best curve fitting on this data shows that  $Y = 2.69e^{0.1105x}$ . This equation shows that when the confining pressure is zero, the tensile strength obtained by the equation is 2.69 MPa, which is a real one. Therefore, this equation can be used for measurement of Is50 when the model is under the confining pressure.

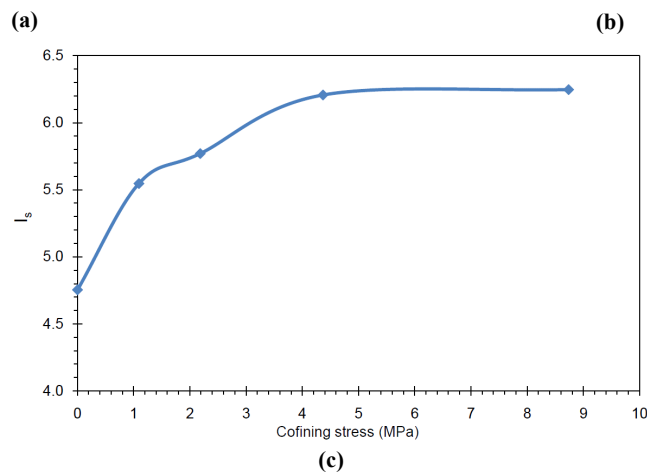
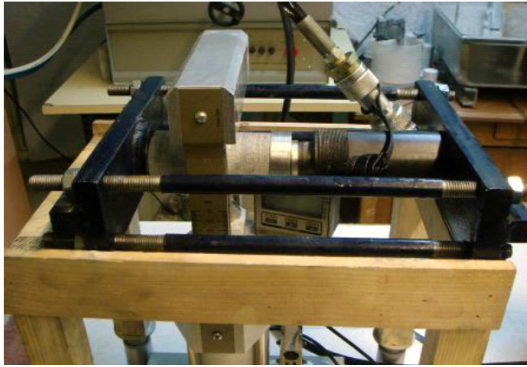


Figure 9. a) Assembly of PLT in the presence of confining pressure, b) typical failure pattern occurring in the samples, c) effect of confining pressure on the point load index for marble.

## References

- [1]. Bazant, Z.P. (2002). Concrete fracture models: testing and practice. *Engineering Fracture Mechanics* 69, 165–205.
- [2] Shah, SP., Swartz, SE. and Ouyang, C. (1995) *Fracture mechanics of concrete*. New York: John Wiley and Sons Inc.
- [3]. Chen, W.F. (1970). Double punch test for tensile strength of concrete. *ACI Materials Journal* 67 (2): 993–995.
- [4]. Mazars, J. (1986). A description of micro- and macroscale damage of concrete structures. *Engineering Fracture Mechanics* 25, 729–737.
- [5]. Protodyakonov, M.M. and Voblikov, V.S. (1957). Determining the strength of rocks on samples of an irregular shape, *Ugol.* 32 (4).
- [6]. Bieniawski, Z.T. (1975). The point-load test in geotechnical practice, *Eng. Geol.* 9 (1): 1-11.
- [7]. Broch, E. and Franklin, J.A. (1972). The point-load strength test, *J. Rock Mech. Min. Sci. Geomech. Abstr.* 9 (6): 669-676.
- [8]. Basu, A. and Kamran, M. (2010). Point load test on schistose rocks and its applicability in predicting uniaxial compressive strength, *J. Rock Mech. Min. Sci.* 47 (5): 823-828.
- [9]. Basu, A., Mishra, D.A., and Roychowdhury, K. (2013). Rock failure modes under uniaxial compression,

- Brazilian, and point load tests”, *Bull. Eng. Geol. Environ.* 72 (3, 4): 457-475.
- [10]. Singh, T.N., Kainthola, A. and Venkatesh, A. (2012). Correlation between point load index and uniaxial compressive strength for different rock types, *Rock Mech. Rock Eng.* 45 (2): 259-264.
- [11]. Chau, K.T. and Wong, R.H.C. (1996). Uniaxial compressive strength and point load strength of rocks, *J. Rock Mech. Min. Sci. Geomech. Abstr.* 33 (2): 183-188.
- [12]. Fener, M., Kahraman, S., Bilgil, A. and Gunaydin, O. (2005). A comparative evaluation of indirect methods to estimate the compressive strength of rocks, *Rock Mech. Rock Eng.* 38 (4): 329-343.
- [13]. Sonmez, H. and Osman, B. (2008). The limitations of point load index for predicting of strength of rock material and a new approach”, *Proceedings of the 61st Geological Congress of Turkey*, 1, 261-262.
- [14]. Sonmez, H., Gokceoglu, C., Medley, E.W., Tuncay, E. and Nefeslioglu, H.A. (2006). Estimating the uniaxial compressive strength of a volcanic bimrock”, *J. Rock Mech. Min. Sci.* 43 (4): 554-561.
- [15]. Sonmez, H., Tuncay, E. and Gokceoglu, C. (2004). Models to predict the uniaxial compressive strength and the modulus of elasticity for Ankara agglomerate, *J. Rock Mech. Min. Sci.* 41 (5): 717-729.
- [16]. Basu, A. and Aydin, A. (2006). Predicting uniaxial compressive strength by point load test: significance of cone penetration, *Rock Mech. Rock Eng.* 39 (5): 483-490.
- [17]. Kahraman, S. and Gunaydin, O. (2009). Effect of rock classes on the relation between uniaxial compressive strength and point load index, *Bull. Eng. Geol. Environ.* 68 (3): 345-353.
- [18]. Kayabal, K. and Selçuk, L. (2010). Nail penetration test for determining the uniaxial compressive strength of rock, *J. Rock. Mech. Min. Sci.* 47 (2): 265-271.
- [19]. Ma, G.W. and Wu, W. (2010). Water saturation effects on sedimentary rocks, *Civil Eng. Res.*, 23, 129131.
- [20]. Heidari, M., Khanlari, G., Torabi Kaveh, M. and Kargarian, S. (2012). Predicting the uniaxial compressive and tensile strengths of gypsum rock by point load testing, *Rock Mech. Rock Eng.* 45 (2): 265-273.
- [21]. Singh, V.K. and Singh, D.P. (1993). Correlation between point load index and compressive strength for quartzite rocks, *Geotech. Geol Eng.* 11 (4): 269-272.
- [22]. Li, D. and Wong, L.N.Y. (2013). Point load test on meta-sedimentary rocks and correlation to UCS and BTS, *Rock Mech. Rock Eng.* 46 (4): 889-896.
- [23]. Haeri, H., Khaloo, A. and Marji, M.F. (2015). Experimental and numerical analysis of Brazilian discs with multiple parallel cracks, *Arab. J. Geosci.* 8 (8): 5897-5908.
- [24]. Haeri, H., Shahriar, K., Marji, M.F. and Moarefvand, P. (2015). The HDD analysis of micro-crack initiation, propagation, and coalescence in brittle substances, *Arab. J. Geosci.* 8 (5): 2841-2852.
- [25]. Tsiambaos, G. and Sabatakakis, N. (2004). Considerations on strength of intact sedimentary rocks, *Eng. Geol.*, 72(3), 261-273.
- [26]. Zhou, Y.X., Xia, K., Li, X.B., Li, H.B., Ma, G.W., Zhao, J., Zhou, Z.L. and Dai, F. (2012). Suggested methods for determining the dynamic strength parameters and mode-I fracture toughness of rock materials, *J. Rock. Mech. Min. Sci.*, 49, 105-112.
- [27]. Ayatollahi, M.R. and Alborzi, M.J. (2013). Rock fracture toughness testing using SCB specimen, *Proceedings of the 13th International Conference on Fracture*, Beijing, China, June.
- [28]. Wei, M.D., Dai, F., Xu, N.W., Xu, Y. and Xia, K. (2015). Three-dimensional numerical evaluation of the progressive fracture mechanism of cracked chevron notched semi-circular bend rock specimens, *Eng. Fract. Mech.*, 134, 286-303.
- [29]. Xu, N.W. Dai, F. Wei, M.D. Xu, Y. and Zhao, T. (2015a). Numerical observation of three dimensional wing-cracking of cracked chevron notched Brazilian disc rock specimen subjected to mixed mode loading”, *Rock Mech. Rock Eng.* 49 (1): 79-96.
- [30]. Lee, S., Lee, S.H. and Chang, Y.S. (2015). Evaluation of RPV according to alternative fracture toughness requirements, *Struct. Eng. Mech.* 53 (6): 1271-1286.
- [31]. Rajabi, M. Soltani, N. and Eshraghi, I. (2016). Effects of temperature dependent material properties on mixed mode crack tip parameters of functionally graded materials, *Struct. Eng. Mech.* 58 (2): 144-156.
- [32]. Yaylaci, M. (2016). The investigation crack problem through numerical analysis, *Struct. Eng. Mech.* 57 (6): 1143-1156.
- [33]. Lin, Q. and Cao, P. (2021). Crack coalescence in rock-like specimens with two dissimilar layers and pre-existing double parallel joints under uniaxial compression, *International Journal of Rock Mechanics and Mining Sciences*, 139: 39-53.
- [34] Lin, Q., Cao, P., Cao, R., Lin, H. and Meng, J. (2020). Mechanical behavior around double circular openings in a jointed rock mass under uniaxial compression, *Archives of Civil and Mechanical Engineering*. 20 (1):33-45.
- [35]. Lin, Q. and Cao P. (2020). Fatigue behavior and constitutive model of yellow sandstone containing pre-existing surface crack under uniaxial cyclic loading, *Theoretical and Applied Fracture Mechanics*, 109: 111-128.

[36]. Lin, Q. and Cao P. (2020). Strength and failure characteristics of jointed rock mass with double circular holes under uniaxial compression: Insights from discrete element method modelling, *Theoretical and Applied Fracture Mechanics*, 109: 77-89.

[37]. Lin, Q. and Cao, P. (2021). Mechanical behavior of a jointed rock mass with a circular hole under compression-shear loading: Experimental and numerical studies, *Theoretical and Applied Fracture Mechanics*, 114: 100-113.

[38]. Kahraman, S., Gunaydin, O. and Fener, M. (2005). The effect of porosity on the relation between uniaxial compressive strength and point load index, *J. Rock. Mech. Min. Sci.* 42 (4): 584-589.

[39]. Potyondy, D.O. and Cundall, P.A. (2004). A bonded-particle model for rock. *International Journal of Rock Mechanics and Mining Sciences*, 41: 1329–1364.

[40]. Palassi, F. and Afzali, M. (2015). Effects of Lateral Confinement on the Results of Point Load Test. Conference: Geohalifax 2009-62nd Canadian Geotechnical Conference At: Halifax, Canada.

## تأثیر فشار محصورکننده بر Is(50) بدست آمده از آزمایش بار نقطه‌ای

وهاب سرفرازی<sup>۱\*</sup> و کاوه عسگری<sup>۲</sup>

۱- بخش مهندسی معدن، دانشگاه صنعتی همدان، همدان، ایران  
۲- بخش مهندسی معدن، دانشگاه شهید باهنر کرمان، کرمان، ایران

ارسال ۲۰۲۱/۰۵/۱۲ پذیرش ۲۰۲۱/۰۸/۰۲

\* نویسنده مسئول مکاتبات: sarfarazi@hut.ac.ir

## چکیده:

در این مقاله تأثیر فشار محصورکننده بر مقاومت کششی بدست آمده از آزمایش بار نقطه‌ای بوسیله کد جریان ذره مطالعه شده است. در مرحله اول مدل عددی توسط نتایج آزمایش برزیلی کالیبره گردید. مقاومت کششی مدل ۲/۵ مگاپاسکال است. آزمایش بار نقطه‌ای در حضور فشار محصورکننده بر مدل‌هایی به ابعاد ۱۵\*۱۵ سانتیمتر انجام شد. فشار محصورکننده ۱۳ مقدار متفاوت دارد که عبارتند از: ۰ MPa، ۰/۰۰۲ MPa، ۱ MPa، ۱/۵ MPa، ۲ MPa، ۲/۵ MPa، ۳ MPa، ۳/۵ MPa، ۴ MPa، ۵ MPa، ۶ MPa، ۹ MPa و ۱۱ MPa. نرخ بارگذاری ۰/۰۰۱ mm/min است. نتایج نشان می‌دهند که تحت تنش نرمال کم، ترک‌های کششی بطور قایم در مدل رشد می‌کنند. تحت فشار محصورکننده زیاد، چندین شکستگی برشی متناطح در مدل توسعه می‌یابد. تعداد ترک‌های برشی به فشار محصورکننده بستگی دارد. همچنین یک رابطه برای تخمین Is(50) تحت فشار محصورکننده ارائه شده است.

کلمات کلیدی: آزمایش بار نقطه‌ای، PFC2D، ترک کششی.